New Approach to Numerical Analysis of the Hall Thruster

Kybeom Kwon[1] and Dimitri N. Mavris[2]
Aerospace Systems Design Laboratory, Georgia Institute of Technology, Atlanta, GA 30332 USA

and

Mitchell L. R. Walker[3]
High-Power Electric Propulsion Laboratory, Georgia Institute of Technology, Atlanta, GA 30332 USA

The design of Hall effect thrusters (HETs) is typically based on empirical methods and experimental data. The complex physics of the HET prohibits the development of numerical analysis tools to aid and ease the design process. To obtain a better design procedure, this study develops an efficient, robust, and self-consistent 1-D numerical tool for HET analysis using a new approach. The numerical results compare with several HETs from 1 kW to 50 kW class. In addition to performance prediction, the analysis tool includes sensitivity analysis and approximation of radial magnetic field distribution from given performance goals.

I. Introduction

HALL effect thrusters (HET) are in increasing demand for space missions. For example, a study conducted by the In-Space Propulsion Technology Program reports that HETs with proper performance capabilities provide significant benefits for cost and performance for Discovery class missions.[1] However, the designs of new HETs have been mostly empirical and experimental.[2-3] Furthermore, designs for HETs have been done for a specific power level without direct consideration of actual missions or practical objectives.

The design of HETs becomes closely related to the design of optimal low-thrust trajectories when transfer missions are included. The introduction of electric propulsion technology provides many advantages, but it also poses many new problems for space mission design. This is because the traditional trajectory design based on chemical rockets where impulse thrust bits are assumed is no longer applicable. In turn, researchers have used newer mathematical methods for low-thrust trajectory optimization. The first actual mission designed by these new methods were European SMART-1's flight to the Moon.[4] Since then, a variety of methods for low-thrust trajectory optimization have been proposed.[5] Because of inherent difficulties in low-thrust trajectory optimization, these methods basically use an ideal electric engine model that has constant efficiency and constant or linear variation of specific impulse with power. Thruster operations with any power inputs are assumed, which is not true for real thrusters. Because of these simplified models, it was difficult to accurately model interactions between thruster and trajectory design, so the two have been decoupled in the past. Although there has been work that incorporates detailed thruster performance into trajectory optimization and mission analysis, it was done with performance of a specific HET, not coupled design for both HET and optimal trajectory.[6]

The use of modern design processes can aid in some of the difficulties of HET design as well as coupled design in the conceptual stage of space missions. Among the recent conceptual design methodologies, design space exploration (DSE) can be used for rapidly assessing the whole design space. The advantages of DSE are that: 1) detailed correlation information between design variables can be obtained, 2) the feasible regions, here the performance envelope, can be identified, and 3) it could provide an environment for further investigations such as optimization, sensitivity analysis, robust design, and probabilistic design. For an efficient DSE, an appropriate numerical analysis tool for HET performance is required. Furthermore, it should be a physics-based tool rather than an empirical one because experimental data is insufficient and the physics involving HET is highly complex and nonlinear.

[1] Graduate Research Assistant, Department of Aerospace Engineering, kybeom.kwon@gatech.edu, AIAA Student Member.
[2] Professor, Department of Aerospace Engineering, dimitri.mavris@ae.gatech.edu, AIAA Associate Fellow.
[3] Assistant Professor, Department of Aerospace Engineering, mitchell.walker@ae.gatech.edu, AIAA Senior Member.

In this paper, a technique to create a physics-based tool to explore the performance design space of the HET is presented. First, existing tools and methodologies are evaluated against a set of required tool criteria. This effort leads to the development of a new physics-based tool. Finally, tool validation results and additional tool capabilities are discussed.

II. Investigation of Existing Tools and Methodologies

A. Criteria for the Required Analysis Tool

In order to identify a proper physics-based analysis tool for the current purpose, the following criteria are proposed:

1) Numerical Efficiency
2) Numerical Robustness
3) Self-Consistency
4) Physics Representativeness

Numerical efficiency is apparently the most important property because a large design space should be explored at a conceptual level of design. If the selected tool is numerically robust in the solution procedure, it is considered as a robust method. However, if it is highly dependent on the initial guesses, it is not considered to be numerically robust. The definition of self-consistency is limited and specific in that there should be no unknowns that have to be set to arbitrary values in the tool. Lastly, physics representativeness is chosen to ensure that the approximate solution provided by the tool should give a reasonable accuracy at a conceptual level.

Among the four criteria, the requirements for the first three should be high and a moderate emphasis on the fourth criterion should be sufficient.

B. Identification of the Required Tool among Existing Tools or Methodologies

Many technical papers have been published on the numerical methods for HET analysis. The numerical methods fall in three major categories: kinetic, continuum/fluid, and hybrid methods. Each tool and methodology has been investigated for its characteristics based on the proposed criteria. Table. 1 shows the result of investigation.

Table 1. Tool identification based on the proposed criteria.

Researcher	Numerical Efficiency (***high***)	Numerical Robustness (***high***)	Self-Consistency (***high***)	Physics Representativeness (***middle***)
Komurasaki et al. (1995)[7]	middle	***high***	low	low
Boeuf et al. (1998)[8]	middle	***high***	low	low
J. Ashkenazy et al. (1999)[9]	***high***	low	low	low
Fruchtman et al. (2000)[10]	***high***	low	low	low
Ahedo et al. (2002)[11]	***high***	low	***high***	***middle***
Subrata Roy et al. (2002)[12]	middle	***high***	low	low
Avi Cohen-Zur et al. (2002)[13]	***high***	low	low	***middle***
L. Dorf et al. (2003)[14]	***high***	middle	low	low
Keidar et al. (2001)[15]	***high***	***high***	low	***middle***
Hybrid Approach[16]	low	***high***	***high***	***high***
Kinetic Approach[17]	very low	***high***	***high***	***high***

Table. 1 is a subjective evaluation based on our experience with the codes. Although each method has its purpose in their applications, it is identified that none meets the proposed criteria simultaneously for the current purpose. As a result, there is a need to develop an appropriate tool for HET analysis.

III. Development of the Intended Tool

A. Ideas to Meet the Criteria

Due to the high computational cost of kinetic and hybrid methods, a 1-D continuum/fluid method is chosen to ensure the numerical efficiency. In order to avoid the singular formulation in an approach using a system of ordinary differential equations (ODEs), each ODE for a specific variable can be solved sequentially while other variables remain constant. Then the convergence can be obtained by iterations, which is called the relaxation method. The most important idea to have numerical robustness and self-consistency is that the solution domain is divided into two regions; collisionless region (presheath region) and collision dominant region (ionization/acceleration region) as shown in Fig. 1.

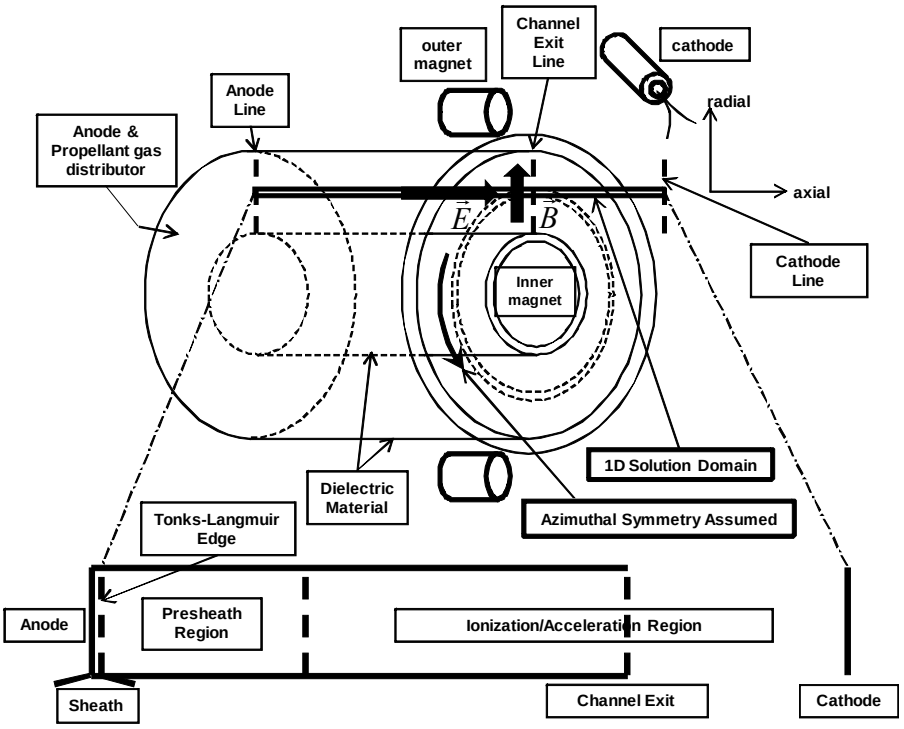

Figure 1. Schematics of analysis domain.

The division of the domain is based on the following observation; at the region near the exhaust where the strength of the radial magnetic field is high, the electron trajectory is almost trapped by the strong radial magnetic field. Closer to the anode, the effect of trapping is decreased since the magnetic field is also lower. Therefore, at the region near the anode, the electrons are almost purely diffused directly toward the anode.

Most of previous methods employing fluid description suffer from a loss of self-consistency by setting an arbitrary boundary values at the anode sheath edge (Tonks-Langmuir edge). In order to be self-consistent, somehow the physics near the anode region must be modeled. Several researchers have noted that positive anode fall can result in discharge extinguishment at low propellant mass flow rate operation.[18] Furthermore, several experimentalists have previously confirmed the existence of negative anode fall.[19-21] In addition, several numerical methods successfully solve the HET operation characteristics with the negative anode fall boundary condition.[18,22] Therefore, the negative anode fall is taken as one of general physical phenomena in HET. In this case, the ion backflow must be provided to meet the Bohm criterion at the anode sheath edge in the presheath region.[23]

The interface linking the two regions should be the point where the ion mean velocity is equal to zero. These two regions are mathematically distinguished mainly by different treatments of the electron momentum equation. The two regions are solved independently and the properties at the common interface must be matched for all dependent variables. The detailed solution strategy will be discussed in the following section, but the idea of treating the anode sheath/presheath region and ionization/acceleration region separately ensures both numerical robustness and self-consistency.

The actual physical phenomenon to which the most careful attention must be given is regarding electron anomalous diffusion. The electron anomalous diffusion has been a hot topic of controversy among HET researchers and it has still not been fully understood. Because it is impossible to resolve the mechanism for anomalous diffusion using the current approach, the most recent experimentally suggested formula is used for the anomalous diffusion.[24] Although Ref. 24 concluded that the electron-wall collisions play a minor role in the anomalous transport, electron-wall collisions must be included to be consistent for electron-wall energy loss rate when solving for electron temperature.

B. Development Strategy

In the anode sheath region, the information on the potential difference between the anode and anode sheath edge ($\varphi_{edge-d} = \varphi_{edge} - \varphi_d$, where φ is the electric potential) is only required as shown in Fig. 2.

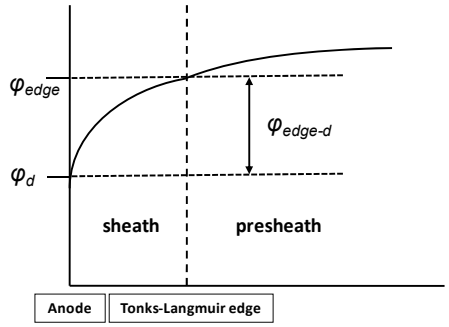

Figure 2. Schematic of electric potential distribution in anode sheath region.

The current balance around the anode is simply current continuity, which means that the discharge current is the sum of thermal, bulk, and displacement currents. Since most currents are carried by electrons at the anode sheath edge[25], the relative potential of plasma body to the anode potential at steady state when the displacement current vanishes is given by[26]

$$e\varphi = -kT_e \ln \frac{I_{discharge}}{I_{thermal+bulk}} \tag{1}$$

where k is the Boltzmann constant, T_e is the electron temperature, and I is the current. Because the bulk electron mean velocity should be the same order of magnitude with thermal velocity in order to have discharge current[25], the plasma current from thermal flux and bulk movement of electrons would be almost twice that of the discharge current. Therefore, Eq. (1) is reduced to the following relation:

$$e\varphi_{edge-d} = kT_e \ln 0.5 \approx 0.6931\, kT_e \tag{2}$$

The governing equations for the presheath region with an assumption of constant electron temperature are given as

$$\frac{d\Gamma_n}{dz} = -S \qquad \frac{d\Gamma_i}{dz} = S \qquad \frac{d\Gamma_e}{dz} = S$$
$$\frac{d(n_e u_i^2)}{dz} = -\frac{en_e}{m_i}\frac{d\varphi}{dz} \tag{3}$$
$$0 = -kT_e \frac{dn_e}{dz} + en_e \frac{d\varphi}{dz}$$

where the subscripts, *n, i,* and *e*, represent neutral, ion, and electron, respectively, n is the number density, u is the mean velocity, $\Gamma = nu$ is the species number flux, z is the axial coordinate variable, and S is the ionization source

term, which is given by $S = n_e n_n \langle \sigma_i v_e \rangle$. The electron energy equation does not need to be solved. The solution procedure is similar to that presented in Ref. 27.

The governing equations for the ionization/acceleration region are given as

$$u_n \frac{dn_n}{dz} = -S \qquad \frac{d\Gamma_i}{dz} = S \qquad \frac{d\Gamma_e}{dz} = S$$

$$n_e(z) = \int_0^z \frac{S(z')dz'}{\left[u_{n,0}^2 + 2\frac{e}{m_i}(\varphi(z') - \varphi(z))\right]^{1/2}} + \frac{n_{e,0}u_{i,0}}{\left[u_{n,0}^2 + 2\frac{e}{m_i}(\varphi_0 - \varphi(z))\right]^{1/2}} \tag{4}$$

$$\frac{d(e\varphi)}{dz} = \frac{m_e \nu_{e,m}}{n_e}\Gamma_e$$

$$\frac{d\varepsilon_e}{dz} = -\frac{3}{5}eE - \frac{3}{5}\frac{n_e \nu_{e,\varepsilon}}{\Gamma_e}\varepsilon_e - \frac{n_e \nu_i}{\Gamma_e}\varepsilon_e$$

where the subscript *0* represents properties at the common interface, *e* is the electrical charge quantity, *m* is the mass, $\nu_{e,m}$ is the electron momentum collision frequency, $\nu_{e,\varepsilon}$ is the electron energy loss frequency, ν_i is the ionization frequency, ε_e is the electron internal energy, and *E* is the electric field. As seen in Eqs. (3) and (4), the electron momentum equation has a different form for each region. The solution procedure is similar to that presented in Ref. 28 and 29. The detailed solution procedure for each region is given in Ref. 30.

In order to match two solutions, all the values of the unknowns from each region must be the same at the matching point. The strategies are as follows:

1) Neutral number density: it is constant and fixed as the one obtained from the given propellant mass flow rate.
2) Ion mean velocity: it is zero at the matching point.
3) Electron mean velocity: it is obtained from the solution of the ionization/acceleration region by solving the electron momentum equation.
4) Electron temperature: it is calculated by solving the electron energy equation in the ionization/acceleration region with a boundary condition of electron temperature at the cathode, which is set to 0.
5) Plasma number density: it is assumed first. After obtaining solutions from the ionization/acceleration region, the electron temperature at the matching point and discharge current are known. In order to update plasma number density at the matching point, the current continuity is employed. The total current at the anode sheath edge is calculated, which allows the plasma number density to be updated using the relation given by

$$\frac{I_d}{eA} = (n_e u_i - n_e u_e)\big|_{edge} = n_{e,m} \exp\left[-\frac{e\phi_{m-edge}}{kT_e}\right]\left[-\sqrt{\frac{kT_e}{m_i}} + \sqrt{\frac{kT_e}{2\pi m_e}}\right] \tag{5}$$

where I_d is the discharge current, *A* is the thruster channel area, and subscript *m* represents properties at the matching point (common interface).

6) Electric potential: it is obtained from the sheath/presheath solution.

By iteratively applying the strategies above to match two solutions, the final converged solution can be obtained. The under-relaxation scheme is implemented to ensure numerical robustness, which is given by

$$V^p = \alpha_{relax} V^p + (1 - \alpha_{relax}) V^{p-1} \tag{6}$$

where *p* is the iteration step, *V* is the dependent variable vector, and α_{relax} is the relaxation coefficient, and for under-relaxation, it has a value between 0 to 1. In conclusion, the proposed method presented in this section possesses self-consistency from the fact that all the dependent variables are determined by the method. The solution procedure is numerically robust by avoiding singular formulation. Furthermore, the method is expected to have no dependence on the initial guesses.

IV. Validation and Results

The proposed formula for the anomalous coefficients is only a function of discharge voltage and those are fixed as constant values over 400 V, which is given as

$$\hat{\alpha}_{ano} = \hat{\alpha}_{ano,\min}\left[1-\exp\left\{A\left(\frac{V_d-400}{400-150}\right)^2\right\}\right]+\hat{\alpha}_{ano,\max},\ where\ A=\log\left(1+\frac{\hat{\alpha}_{ano,\max}-\hat{\alpha}_{ano,\min}}{\hat{\alpha}_{ano,\min}}\right) \tag{7}$$

where $\hat{\alpha}_{ano,in}$ and $\hat{\alpha}_{ano,out}$ are the inverses of the anomalous coefficients inside and outside the channel. The minimum and maximum values inside the channel are 100 and 160, and 50 and 80 outside the channel. Furthermore, the result is derived based on the experiments only from the comparison with a 5-kW HET. Thus, it is also required to check the general applicability of Eq. (7) in validation. This is performed by treating the anomalous coefficients as free parameters with their value ranges and investigating their effects on the results.

A. Definition of Performance Metrics

For the validation purpose, the performance metrics are defined as follows: Thrust includes neutral contribution and it is defined as

$$T = \dot{m}_{i,c}u_{i,c} + \dot{m}_{n,c}u_{n,c} \tag{8}$$

where $\dot{m}$ is the mass flow rate and subscript c represents properties at the cathode line. The anode specific impulse is introduced as

$$I_{sp,ano} = \frac{T}{\dot{m}_a g_0} \tag{9}$$

where $\dot{m}_a$ is the anode mass flow rate and g_0 is the gravitational acceleration at the Earth's surface. The anode efficiency is also introduced as

$$\eta_{ano} = \frac{T^2}{2\dot{m}_a P_d} \tag{10}$$

where P_d is the discharge power, which is defined as $V_d \times I_d$. Total power required to sustain the discharge can be expressed as

$$P_{tot} = P_d + P_{cath} + P_{mag} \tag{11}$$

where P_{cath} is the power required to operate the cathode and P_{mag} is the power required to produce magnetic field. If the specific impulse and efficiency include the cathode mass flow rate, those are termed as total specific impulse and total efficiency, respectively. For these total quantities as well as total power, additional inputs are required such as

1) Percentage of $\dot{m}_c$ based on $\dot{m}_a$ (%): this is termed as pmc
2) Percentage of P_{cath} based on P_d (%): this is termed as ppc
3) Percentage of P_{mag} based on P_d (%): this is termed as ppm

where $\dot{m}_c$ is the cathode mass flow rate. Therefore, if those inputs are provided, the following total quantities can be calculated.

1) Total specific impulse

$$I_{sp,tot} = \frac{T}{\dot{m}_{tot} g_0} = \frac{T}{(\dot{m}_a + \dot{m}_c) g_0} = \frac{T}{(1+0.01pmc)\dot{m}_a g_0} = \frac{I_{sp,ano}}{(1+0.01pmc)} \tag{12}$$

2) Total efficiency

$$\eta_{tot} = \frac{T^2}{2\dot{m}_{tot} P_{tot}} = \frac{T^2}{(1+0.01pmc)(1+0.01ppc+0.01ppm)2\dot{m}_a P_d} = \frac{\eta_{ano}}{(1+0.01pmc)(1+0.01ppc+0.01ppm)} \tag{13}$$

3) Total power

$$P_{tot} = P_d + P_{cath} + P_{mag} = P_d + 0.01(ppc + ppm)P_d = (1+0.01ppc+0.01ppm)P_d \tag{14}$$

B. Classification of Solutions Obtained From the Developed Method

The developed method has a convergence criterion, i.e., if the normalized sum of relative changes in plasma properties (variable name in the code: ERRORL) is less than the pre-specified tolerance (variable name in the code: CONV), which is usually very small value, for example, 1e-8), then the code stops calculation and the plasma properties at that moment are taken as the solution. The method also employs the maximum iteration number (variable name in the code: ITMAX) for the case of non-convergent but oscillatory solution.

1) Case I: ERRORL ≤ CONV – Success

The solution procedure is considered as successful and the converged solution is obtained. Typical convergence histories of error and performance metrics are shown in Fig. 3. In particular, the initial half part of the error history shows oscillation and a little growth. Since the initial guesses of electron temperature and plasma number density are quite low, it can be thought that the discharge is established during that part of the history by resembling time-accurate startup transient phenomena.

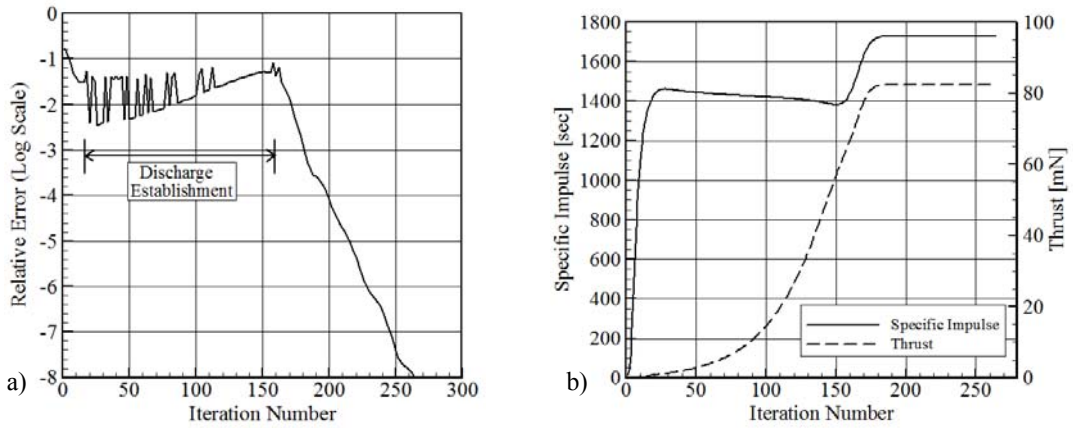

Figure 3. Convergence history of case I: a) error, b) specific impulse and thrust.

2) Case II: ERRORL > CONV and ITMAX reached – Success

In this case, the solution procedure is also considered as being successful, but the error history exhibits oscillatory behavior. Although the relative error does not reach the pre-specified tolerance, CONV, the performance metrics show convergent behavior. These characteristics are shown in Fig. 4. Because the oscillatory error behavior is identified well after pseudo-discharge establishment as explained in Case I, it can be inferred that main discharge characteristics are achieved. However, in this case, it is required to take averages on values of performance parameters during some last iteration steps, for example, about 100 iteration steps.

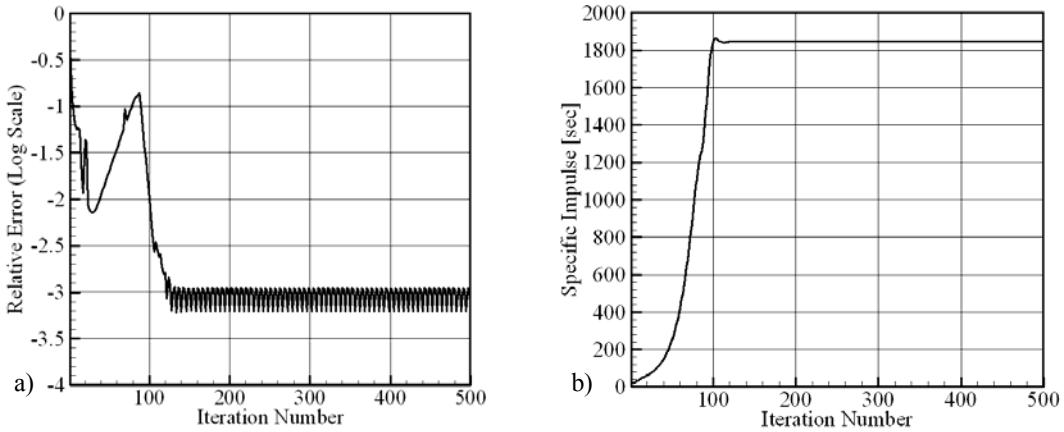

Figure 4. Convergence history of Case II: a) error, b) specific impulse.

3) Case III: Low plasma number density at the matching point – Fail

The plasma number density at the matching point is updated at every iteration step by means of Eq. (5). The plasma number density at the matching point is first guessed at low value, for example, $10^{16}\ \#/m^3$. If consecutive updates during first some iteration steps yield values lower than the first guessed value, two cases are observed. First, it decreases initially and then increases over the first guessed value. The consequence of this process results in Case I or Case II, which is a successful solution. Second, it keeps decreasing and reaches a negative value. Thus, the solution process cannot proceed further and produce no performance outputs. The pseudo-discharge characteristic is not observed, either. This is considered as a failure case. The reason of this seems to be due to low propellant mass flow rate, not enough discharge voltage, or insufficient electron diffusion.

4) Case IV: Presheath region length < length of one computational grid cell – Fail

If the calculated presheath region length during iterations is less than the length of one computational grid cell, the solution process also cannot yield any performance output. The reason of this is that the magnetic field strength in the region near the anode is relatively too high. As a result, the presheath region collapses in very thin region near the anode, which cannot be solved by current macroscopic scale method. This is actually not a failure case. The developed method simply cannot recognize a noticeable presheath region in the macroscopic scale. However, in framework of the developed method, noticeable presheath existence in the HETs should be guaranteed. The magnetic field profile should have sufficiently low radial magnetic field strength in the region near the anode. Because the magnetic field profile may be constructed in this way in the view of design, this case is classified as a failure case to avoid large magnitude of magnetic field strength near the anode region.

5) Case V: Positive electron mean velocity at the cathode – Fail

In this case, the electron mean velocity at the cathode is positive during iteration steps, which means that electrons get away from the thruster. If this happens, the electron temperature in the region near the cathode will be negative, which prevents from obtaining solution. There are several possibilities for this occurrence. First, the thruster might require more voltage difference between the anode and the cathode, since the electric potential profile exhibits decreasing and increasing behavior near the cathode. Second, electron mobility might be not enough due to low electron temperature.

6) Case VI: Presheath region length > thruster device length – Fail

Basically, the reason seems to be similar to those for the Case V. Especially, the fact that electron temperature at the matching point might be too low (cold plasma) causes this failure.

Based on observations of many numerical experiments on failure cases, Case III is the most dominant factor, which clearly indicates that certain input combinations cannot achieve discharge phenomenon for the given thruster. Case III through Case VI stops the solution procedure. Because these are occurring during the iteration steps, it should be checked whether the exact causes of failure cases is physical or numerical. This requires intensive validation with a variety of existing thrusters.

C. Validation with the SPT-100

The specified ranges of the anomalous coefficients are explored by numerical experimentation. Lower and upper bounds of $\hat{\alpha}_{ano,in}$ and $\hat{\alpha}_{ano,out}$ are given previously. In order to conduct numerical experiment, six level full factorial design is used to create an experiment table, which results in a total of 36 runs. Each numerical exploration

is performed for each anode mass flow rate of the SPT-100 experimental data in Table. V of Ref. 31. Fig. 5 shows grids to visualize success/fail cases of the solutions as well as probability of success for each mass flow rate case based on classification given in previous section.

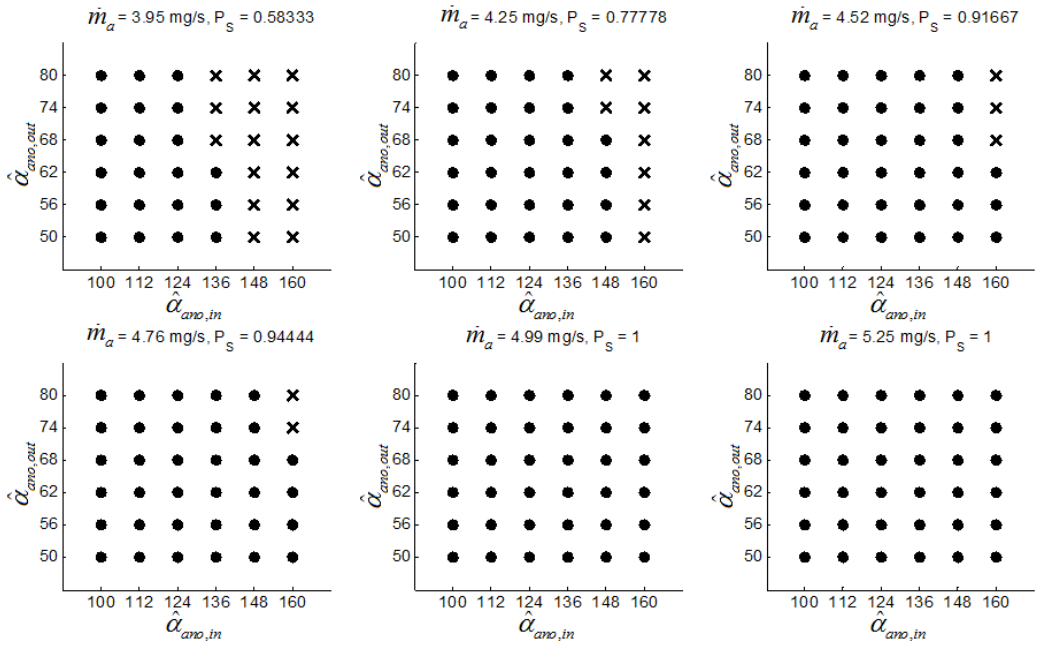

Figure 5. Visualization of numerical experimentation (dot – success, cross – fail).

As the anode mass flow rate decreases, more failed cases are observed. In general, the developed method can produce solutions at higher values of the anode mass flow rate for entire ranges of the anomalous coefficients. In reality, as the anode mass flow rate increases, maximum electron temperature would also increase. Thus, it could start to cause thermal and structural problems of the thruster. It can be also inferred that the higher electron anomalous diffusion is required for the thruster to work in case of lower anode mass flow rate operation, which indicates that if the electron anomalous diffusion are not enough, the discharge could not be established.

Response surface equations through regression with the results of numerical experimentation can be used to find the values of the anomalous coefficients closely matching the experimental data. Standard least square method is used to create response surface equations. In order to find these anomalous coefficient values, optimization strategy is required. The optimization performance index should be differences between values from the response surface equations and experimental values, which can be expressed as sum of square errors. Thrust, discharge current, total specific impulse, and total efficiency are taken as the required responses to be matched for this purpose.

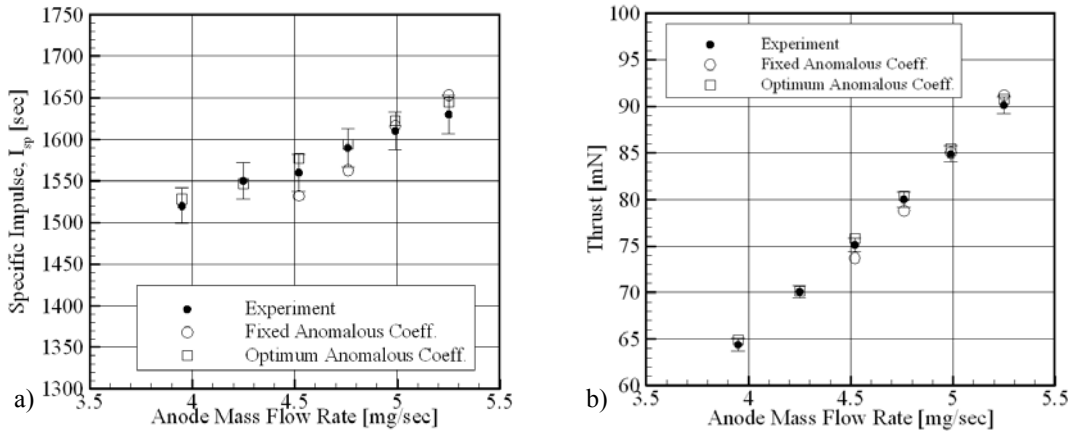

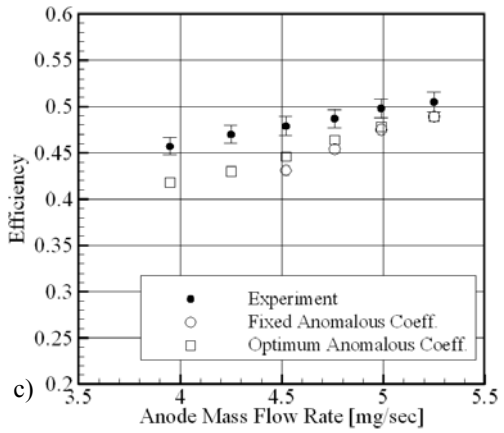

c)

Figure 6. Comparison of experiments, fixed and optimum anomalous coefficients a) total specific impulse, b) thrust, and c) total efficiency.

The optimization is conducted for all of the anode mass flow rate cases. Comparisons of total specific impulse, thrust, and total efficiency for fixed and optimum anomalous coefficients are shown in Fig. 6. Note that the developed method can produce solutions for the anode mass flow rates of 3.95 and 4.52 mg/s, which could not be obtained with the fixed values of the anomalous coefficients using the proposed formula. This is due to increase of axial electron diffusion. Utilizing optimization strategy yields very accurate predictions for the total specific impulse and the thrust. However, prediction of the total efficiency produces a little lower value than the experimental data for all cases. Nonetheless, it can be concluded that the use of optimum anomalous coefficients results in successful validation results for all validation points as well as for the cases of lower anode mass flow rate when compared to the fixed anomalous coefficient cases.

Interesting fact is that $\hat{\alpha}_{ano,in}$ increases as the anode mass flow rate increases as shown in Fig. 7, while $\hat{\alpha}_{ano,out}$ does not have much impact on performance parameters. The reason of this fact might be the effect of the cathode mass flow rate fraction as also shown in Fig. 7. The cathode mass flow rate fraction increases as the anode mass flow rate is decreased. It is inferred that the anomalous coefficient inside the channel and the cathode mass flow rate fraction are positively correlated.

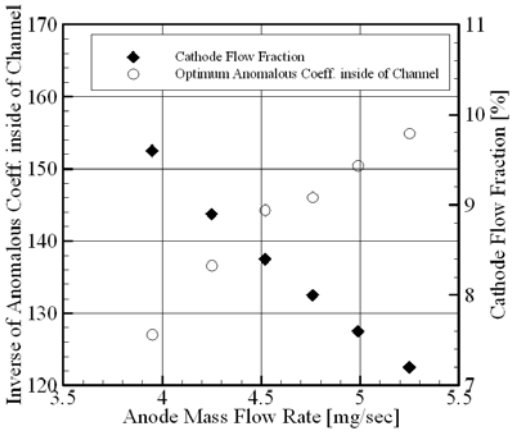

Figure 7. Variation of $\hat{\alpha}_{ano,in}$ and cathode mass flow rate fraction with anode mass flow rate.

D. Pseudo-Validation with the T-220 HET

The T-220 is a 10-kW HET and its outer diameter is 220 mm as identified by its name. In order to validate the developed method with experimental data of the T-220, the radial magnetic field distribution is required, which is not available. However, if the Design Of Experiment (DOE) is utilized as done in previous section, approximate radial magnetic field distribution can be obtained. The approach is a kind of reverse engineering process and the

process can be generalized for other HETs as well. This is the reason why the process is called "Pseudo-Validation."

It is evident that pseudo-validation necessarily increases the number of numerical experiments because parameters characterizing the radial magnetic field distribution should be incorporated in the DOE. The radial magnetic field distribution along the thruster axial coordinate up to the cathode in the developed method can be completely determined by three parameters such as B_{max}, B_{cath}, and magnetic field shape coefficient inside the channel, which is denoted by K. B_{max} and K completely determine the distribution inside channel by Eq. (15).

$$B(z) = B_{\max} \exp\left[-K\left(\frac{z}{L} - 1 \right)^2 \right] \tag{15}$$

B_{max} and B_{cath} also determine the distribution outside the channel by the assumption of linear distribution. Therefore, variables in the DOE consist of three parameters for the magnetic field distribution and two parameters for the anomalous coefficients. The ranges of magnetic field variables are given in Table. 2. In actual numerical experimentation, ΔB, difference between B_{max} and B_{cath}, is taken instead of B_{max} because B_{max} must be greater than B_{cath}, and it is more preferable to have square space in terms of the DOE. The 4 level full factorial design is created, which results in total 1024 runs.

Table 2. Ranges of radial magnetic field parameters.

	B_{max} [T]	ΔB [T]	B_{cath} [T]	K
Lower Limit	0.015	0.005	0.010	12
Upper Limit	0.031	0.013	0.018	20

The experimental data is taken from Ref. 32. In the optimization to find optimum values, the normalized values in terms of median of each variable range are used and the optimization performance index is chosen to be the sum of square errors between the experimental data and the calculated value. Because regression equations are all quadratic and objective function is also quadratic, only one step is required to find optimum values regardless of initial conditions. The optimization results are shown in Table. 3 with the comparison with the experimental data and corresponding errors. The comparisons show great accuracy and the errors are all within 2%.

Table 3. Validation Results for the T-220

Parameters	Experimental Results	Numerical Results	Error (%)
T [mN]	512	507	- 0.97
$I_{sp,tot}$ [s]	2356	2348	- 0.34
η_{ano} [%]	65	64	- 1.54
η_{tot} [%]	57	56	- 1.75
I_d [A]	20	20	0
P_{tot} [kW]	10.394	10.462	+ 0.65
B_{max} [G]		**196**	
B_{cath} [G]		**119**	
K		**12.128**	
$\hat{\alpha}_{ano,in}$		**100.00**	
$\hat{\alpha}_{ano,out}$		**80.00**	

The maximum magnetic field strength is calculated as 196 Gauss, which is 36 Gauss more than that of the SPT-100. The magnetic field strength at the cathode is lower than that of the SPT-100. The inverse of anomalous

coefficient inside the channel reaches lower bound. On the other hand, the inverse of anomalous coefficient outside the channel reaches the upper bound. Fig. 8 shows the approximate radial magnetic field distribution from the optimization results.

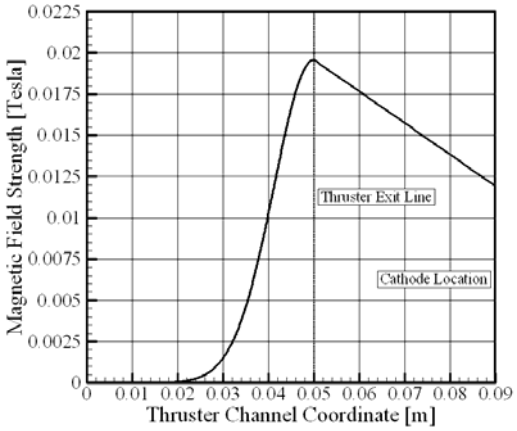

Figure 8. Approximate radial magnetic field distribution of the T-220.

Because the optimization results on the anomalous coefficients are still arbitrary, further investigation on the effects of their variations is required so that obtained approximate radial magnetic field distribution is accepted with quantitative confidence. In order to obtain quantitative confidence of choosing the optimum values of the magnetic field distribution parameters, an MC simulation is conducted. The 100 × 100 random values for the anomalous coefficients are generated and performances are calculated using performance response surface equations while keeping the obtained approximate magnetic field distribution. Table. 4 shows the results. The variations with the anomalous coefficients for the thrust, specific impulse and efficiencies are small, which is less than 7%. The discharge current and power show a little large variance, which is about 17%. However, if mean values of those metrics and their distributions are considered, the difference is very small. In conclusion, the approximate magnetic field distribution found from the current method could be accepted with favorable confidence.

Table 4. Performance metric distribution at optimum magnetic field distribution.

	Thrust [mN]	I_{sp} [sec]	η_{ano}
Distribution	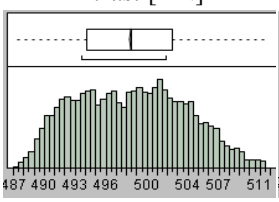	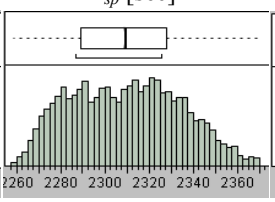	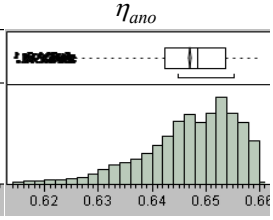
Experiment	512	2356	0.65
Mean	498.42	2309.44	0.647
Standard Deviation	5.27	24.42	0.0086
Range (max. – min.)	24.05 (4.8%)	111.48 (4.8%)	0.0456 (7.0%)
	η_{tot}	I_d [A]	P_{tot} [kW]
Distribution	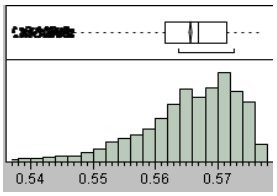	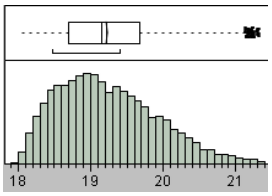	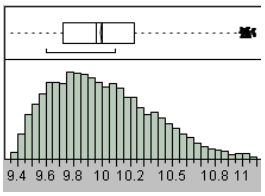
Experiment	0.57	20	10.394
Mean	0.566	19.22	10.00
Standard Deviation	0.0075	0.667	0.347
Range (max. – min.)	0.0398 (7.0%)	3.333 (17.3%)	1.733 (17.3%)

E. Pseudo-Validation with the NASA-457M HET

The NASA-457M HET is a 50 kW class HET. Outer diameter of the NASA-457M is 457 mm as also identified by its name. Validation of the developed method with experimental data of the NASA-457M is a lot more difficult because geometric information is also not available from literatures as well as the radial magnetic field distribution due to the same ITAR regulations. Thus, because the outer diameter is specified, other required geometries are obtained based on Fig. 1 of Ref. 33. Since the picture of the NASA-457M is taken with slant angle to the left, consideration of this effect is required to obtain close estimation.

In order to validate the developed method with estimated geometry, the same approach is taken for "Pseudo-Validation." The variables and their ranges for the DOE are the same as those for the T-220. However, in this case, based on the DOE experiences from the SPT-100 and the T-220, another DOE design strategy is applied to reduce the DOE run time, which is a combination of the Central Composite Design (CCD) and the Latin Hypercube Sampling (LHS). The CCD has advantages of covering the extremes of the concerned space and minimizing the extrapolation. However, as the size of the space becomes large, many experimental cases might not have converged solutions due to emphasis on the extremes. On the other hand, the LHS has rich samplings on the interior of the space. As a result, higher accuracy can be obtained on the interior design space. This advantage of the LHS reduces the accuracy on the edges of the space. Thus, combination of these two design methods is expected to yield a reasonable DOE table. For the given five variables, the CCD produces 43 runs. Additional 157 runs are created by the LHS, which makes the total of 200 runs.

The experimental data is taken from Ref. 33. In Ref. 33, the experimental data by varying the anode mass flow rate from 15 to 93 mg/s and the discharge voltage from 300 to 650 V over a range of input powers from 9 to 72 kW is given. Among these data, four experimental points are selected for the validation. The anode mass flow rate and the cathode mass flow rate for all points are 74.3 mg/s and 7.5 mg/s, respectively. The resultant percentage of the cathode mass flow rate (pmc) is then calculated as 10.09 %. The results of the DOE for the discharge voltage of 300 V show 116 failure cases out of total 200 cases. For the discharge voltage of 402 V, only four failure cases occur. The DOE for other two discharge voltage cases of 500 V and 649 V doesn't have any failure cases. This somewhat coincides with what's encountered for the SPT-100. For the current case, low discharge voltage causes the large number of failure cases. This means that the discharge voltage is also related to the anomalous electron diffusion.

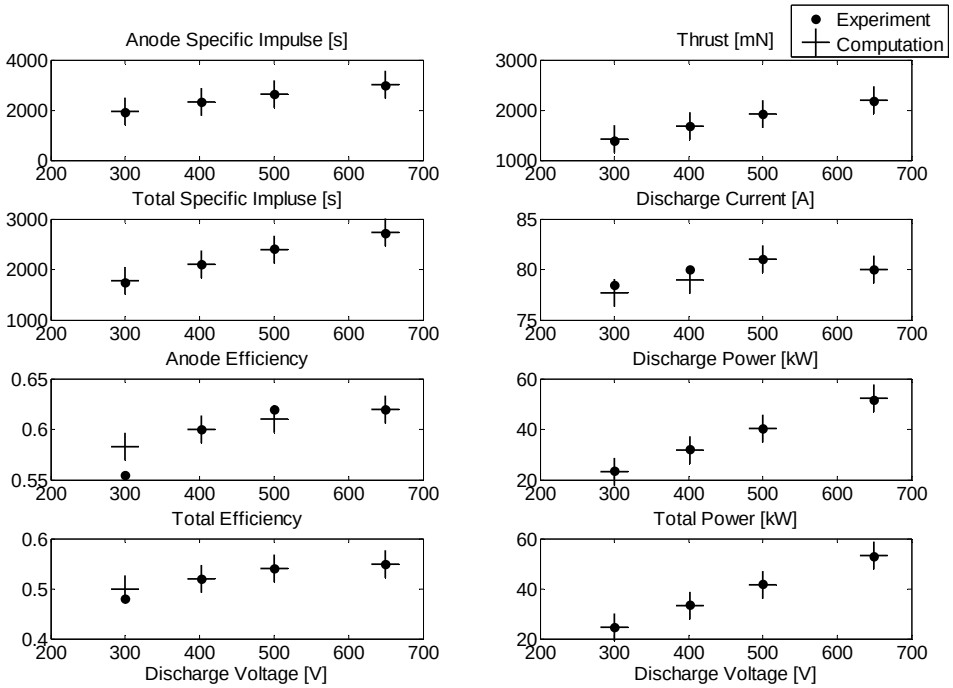

Figure 9. Performance validation for the NASA-457M.

It is assumed that the same magnetic field distribution is typically used for a specific thruster. This can be also deduced from the experimental data. The power required for the magnetic field generation and the cathode operation are calculated as 1.196, 1.355, 1.302, and 1.213 kW for 300, 402, 500, and 649 V, respectively. It is clear

that there is not much difference for electric magnet power consumptions with the same cathode mass flow rate for each voltage case. Thus, it is required to have similar magnetic field distribution for all 4 voltage cases. In the optimization process, this can be done by solving one optimization problem with three global variables for magnetic field distribution and 8 anomalous coefficients. The performance index is expanded to match all metrics for all voltage cases. Figs. 9 and 10 shows the results of the optimization strategy.

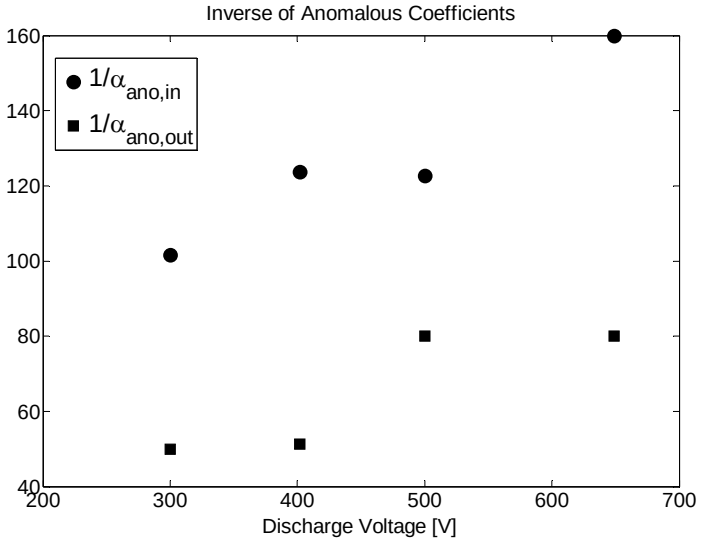

Figure 10. Variations of anomalous coefficients.

The accuracy on the performance metrics is high and the resultant magnetic field distribution is plotted in Fig. 11. Based on the anomalous coefficient variation, it is highly likely that the higher anomalous electron diffusion occurs as the discharge voltage decreases with the same magnetic field distribution. This indicates that higher discharge voltage has negative impact on the anomalous electron diffusion. This behavior of the anomalous electron diffusion is also observed in Ref. 24, which shows that the anomalous coefficient increases as the discharge voltage decreases below 400 V.

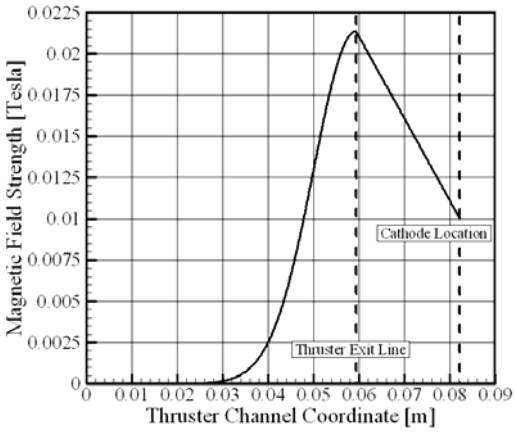

Figure 11. Approximate radial magnetic field distribution of the NASA-457M.

Note that the developed method does not incorporate the effect of multiply-charged ions. The obtained approximate radial magnetic field distribution in Fig. 11 is the one with the assumption of singly-charged ions. Ref. 33 suggests that the effect of multiply-charged ions becomes significant for over 20 kW of discharge power or over 30 A of the discharge current. Thus, this validation can be thought as an approximation of the actual thruster with less confidence that the SPT-100 or the T-220. However, the effect of multiply-charged ions may be incorporated in the developed method by using the method proposed in Ref. 34. In order to prove this possibility, the numerical

experiment is done with the experimental data given in Ref. 33. The experimental data, prediction data by Ref. 34 and the data from the current method are shown in Table. 5. For the calculation, the anomalous coefficients and the magnetic field distribution obtained from Figs. 10 and 11 are used.

Table 5. Effect of Multiply-Charged Ions

Parameters	Experimental Data[33]	Prediction[34]		Current Method
		Multiply-Charged	Singly-Charged	
$\dot{m}_a$ [mg/s]	86.4	88.8	101	86.4
V_d [V]	500	500	500	500
I_d [s]	100	100	100	95.3
$I_{sp,ano}$ [s]	2750	2768	2622	2665

As seen in Table. 5, the singly-charged case achieves approximately 100 s less anode specific impulse than that of multiply-charged ion case. The results of the current method show the same trend as the experimental data. Thus, if the proposed method for the effect of multiply-charged ions in Ref. 34 is incorporated, it is expected that a more confident approximation can be obtained. In conclusion, the developed method can be still used as an effective method for high power HETs.

V. Additional Capabilities of the Developed Tool

A. Sensitivity Studies for the SPT-100

The purpose of the SPT-100 sensitivity studies is to investigate the sensitivities of the performance metrics when varying each specific variable while the other variables remain constant. The sensitivity analysis is usually performed at a known design point to investigate response variations around that design point. Things of interest are the magnitude and direction of the response variation. In this case, the design operation point of the SPT-100 is taken as a known design point. Table. 6 shows the variables of concern and their ranges.

Table 6. Variables and Ranges

Variable	Min.	Max.
Inner Radius [cm]	0.3	0.4
Channel Width [cm]	1	2
Device Length [cm]	3.5	4.5
Cathode Location [cm]	1.5	2.5
Discharge Voltage [V]	251	351
B_{cath} [G]	120	140
ΔB [G]	20	40
K	12	20

The anomalous coefficients inside and outside the channel are assumed to be those at the design point obtained in the SPT-100 validation. The variation of each variable is centered around the design operation point. The range of each variable in this sensitivity study is relatively small, otherwise the assumption of fixed anomalous coefficient values is not valid.

The parametric study is done by varying each variable value in the corresponding range and the results are shown in Fig. 12. The responses of concern are thrust, total specific impulse, total efficiency, and discharge current. The vertical dotted lines correspond to the SPT-100 design operation point for each variable. The triangles indicate the sensitivities at the current variable values. That is the value of the first derivative of the response with respect to the variable. The direction indicates the sign of the first derivative and the size indicates its magnitude. The most influential variables are the inner radius, the outer radius, and the discharge voltage. The increases of responses with the increase of the inner radius and the decreases with the increase of the outer radius are caused mainly by the reduced thruster channel volume, which increases the neutral number density at the given anode mass flow rate. Increasing the maximum magnetic field strength results in negative effects on the performance metrics, but the discharge current is also reduced. Interestingly enough, the response variations with each variable are in the same direction, increasing or decreasing except for relatively small variations of the device length, the magnetic field strength at the cathode, and the magnetic field shape coefficient.

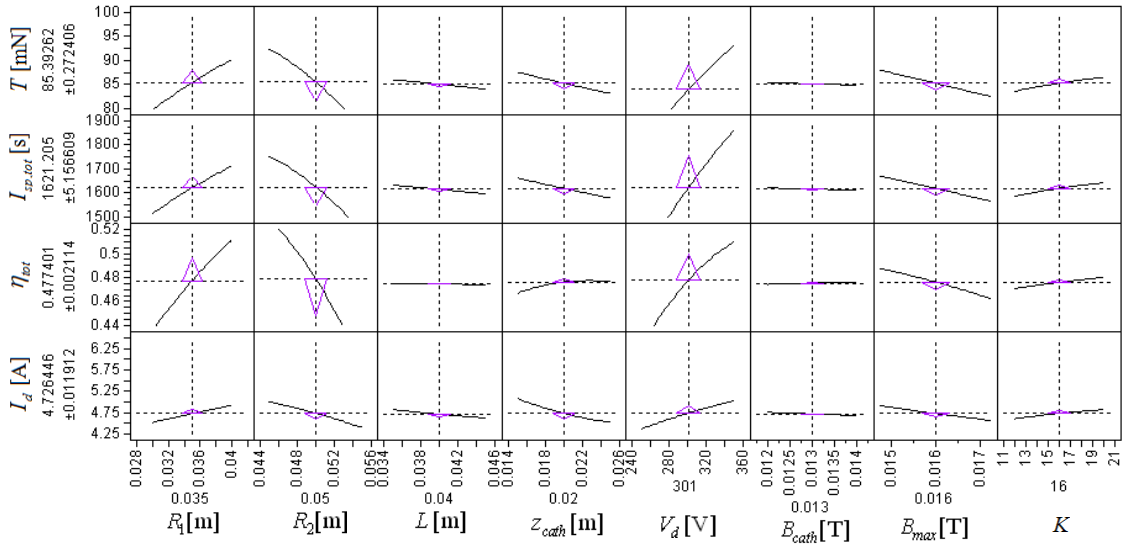

Figure 12. Sensitivity analysis results around the SPT-100 design operation point.

B. Approximation of Radial Magnetic Field Distribution with Given Performance Goals

In this section, we discuss how the radial magnetic field distribution can be approximated with the developed method when performance goals of a specific HET are given. In order to show this capability, the P5 HET is considered. Because the radial magnetic field distribution of the P5 is not restricted by the ITAR regulations, the precise magnetic field distribution can be obtained.[2] The actual radial magnetic field distribution at the design operation point has the following characteristics: 1) B_{max} is 107 G and B_{cath} is 39 G, 2) the location of B_{max} does not coincide with thruster exit line, and 3) the location of B_{max} is approximately 2.62 cm from the anode line while the channel length is 3.81 cm.

The developed method also has the capability to deal with the given radial magnetic field distribution. The analysis of the P5 at the design operation point is attempted. However, the developed method shows a failure case with the given radial magnetic field distribution. The failure case corresponds to Case IV in section IV, which indicates that the presheath region length is smaller than the length of one grid cell. As explained before, this is because the radial magnetic field strength in the region near the anode is relatively high. This means that the developed method does not detect the noticeable presheath existence for the P5.

Now a different perspective is considered. A situation is assumed such that there is a given HET geometry and there are also performance goals designers want to obtain for this thruster. The question is what radial magnetic field distribution is required to produce those performance goals with an additional assumption that structure of the necessary radial magnetic field distribution follows the one assumed in the developed method. In other words, the objective is to find the required B_{max}, B_{cath}, and K. Thus, the P5 becomes a given thruster and the experimental data of its performance metrics become performance goals. If the same method used for the T-220 validation is used, the required radial magnetic field distribution parameters are expected to be found. Since the anomalous coefficients are still arbitrary, those are included as before. The ranges for each variable are selected based on power level of the P5, which is shown in Table. 7.

Table 7. Ranges of magnetic field parameters for the P5.

	B_{max} [T]	ΔB [T]	B_{cath} [T]	K
Lower Limit	0.005	0.005	0.002	1
Upper Limit	0.015	0.013	0.008	16

The 4 level factorial design is created for ΔB, B_{cath}, K, $\hat{\alpha}_{ano,in}$, and $\hat{\alpha}_{ano,out}$. Thus total 1024 runs are executed and those are found using the same method. Table. 8 shows the results. The results of performance metrics calculated from the optimization are very close to experimental performance data. B_{max} is calculated as 120 Gauss, which is slightly higher strength than actual one.

Table 8. Results of finding candidate radial magnetic field distribution.

Parameters	Experimental Results[2]	Numerical Results	Error (%)
T [mN]	178	180	+ 1.12
$I_{sp,tot}$ [s]	1683	1696	+ 0.77
η_{ano} [%]	51	50	- 1.96
η_{tot} [%]	-	47	-
I_d [A]	10.4	10.6	+1.92
P_{tot} [kW]	3.12	3.18	+ 1.92
B_{max} [G]		**120**	
B_{cath} [G]		**80**	
K		**7.01**	
$\hat{\alpha}_{ano,in}$		**114.26**	
$\hat{\alpha}_{ano,out}$		**79.48**	

Figure 13 shows the actual and candidate radial magnetic field distribution. The candidate distribution has lower magnetic field strength in the most of region inside the channel and higher magnetic field strength in other region than the actual one.

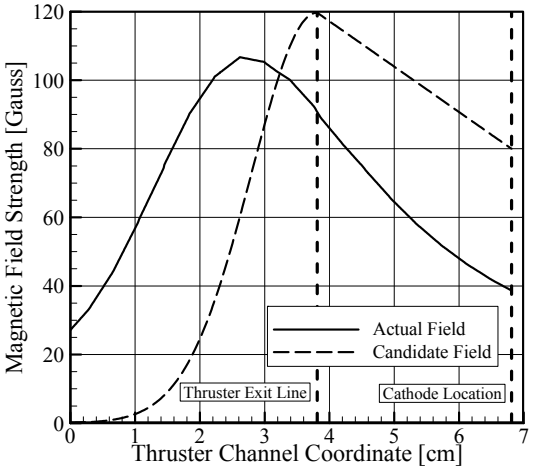

Figure 13. Actual and candidate radial magnetic field distribution of the P5.

In conclusion, it is expected that the procedure established through the validation can be used quite effectively to obtain an approximate magnetic field distribution for a specific thruster geometry to achieve the given performance goals.

VI. Conclusion

A new approach of characterizing HET plasma physics is given and intensive validation for newly developed method is provided. In addition, a sensitivity analysis and approximation of proper radial magnetic field distribution for a given thruster to obtain desired performance characteristics are provided. Based on these validations the developed method can be used as a conceptual design tool for new HETs. This will greatly reduce uncertain design space at the inception of design procedure by providing performance envelope and performance characteristics in the given design space. As a result, this work should aid current design procedures and reduce development cost. In addition, simultaneous design optimization of the HET and associated optimal low-thrust trajectory is expected to reduce preliminary space mission design cycles.

References

[1]Oh, D. "Evaluation of Solar Electric Propulsion Technologies for Discovery Class Missions," AIAA-2005-4270, *41st AIAA Joint Propulsion Conference*, Tucson, AZ, 10-13 July 2005.

[2]Frank Stanley Gulczinski III, "Examination of the Structure and Evolution of Ion Energy Properties of a 5kW Class Laboratory Hall Effect Thruster at Various Operational Conditions," Ph. D. Dissertation, School of Aerospace Engineering, The University of Michigan, Ann Arbor, MI, 1999.

[3]Leonard Biagioni, Massimo Saverdi, and Mariano Andrenucci, "Scaling and Performance Prediction of Hall Effect Thrusters," AIAA-2003-4727, *39th AIAA/ASME/SAE/ASEE Joint Propulsion Conference and Exhibit*, Huntsville, AL, 20-23 July 2003.

[4]Racca, G. D., Foing, B. H., and Coradini, M., "SMART-1: The First Time of Europe to the Moon," *Earth, Moon and Planets*, Vol. 85, 2001.

[5]Kristina Alemany, and Robert D. Braun, "Survey of Global Optimization Method for Low-Thrust, Multiple Asteroid Tour Missions," AAS 07-211, 2007.

[6]David Manzella, David Oh, and Randall Aadland, "Hall Thruster Technology for NASA Science Missions," AIAA-2005-3675, *41st AIAA Joint Propulsion Conference*, Tucson, AZ, 10-13 July 2005.

[7]K. Komurasaki, and Y. Arakawa, "Two-Dimensional Model of Plasma Flow in a Hall Thruster," *Journal of Propulsion and Power*, Vol. 11, No. 6, 1995, pp. 1317-1323.

[8]J. P. Boeuf, L. Garrigues, and L. C. Pitchford, "Modeling of a Magnetized Plasma: The Stationary Plasma Thruster," *Electron Kinetics and Application of Glow Discharge*, 1998, pp. 85-100.

[9]J. Ashkenazy, A. Fruchtman, Y. Raitses, and N. J. Fisch, "Modeling the Behavior of a Hall Current Plasma Accelerator," *Plasma Physics and Controlled Fusion*, Vol. 41, 1999, pp. A357-A364.

[10]A. Fruchtman, N. J. Fisch, and Y. Raitses, "Hall Thruster with Absorbing Electrodes," AIAA-2000-3659, *36th AIAA/ASME/SAE/ASEE Joint Propulsion Conference*, Huntsville, AL, 17-19 July 2000.

[11]E. Ahedo, P. Martinez Cerezo, and M. Martinez-Sanchez, "One-Dimensional Model of the Plasma Flow in a Hall Thruster," Physics of Plasmas, Vol. 8, No. 6, June 2001, pp. 3058-3068.

[12]Subrata Roy, and B. P. Pandey, "Numerical Investigation of a Hall Thruster Plasma," *Physics of Plasmas*, Vol. 9, No. 9, Sept. 2002, pp. 4052-4060.

[13]Avi Cohen-Zur, Amnon Fruchtman, Joseph Ashkenazy, and Alon Gany, "Analysis of the Steady-State Axial Flow in the Hall Thruster," *Physics of Plasmas*, Vol. 9, No. 10, Oct. 2002, pp. 4363-4374.

[14]L. Dorf, and V. Semenov, "Anode Sheath in Hall Thrusters," *Applied Physics Letters*, Vol. 83, No. 13, Sept. 2003, pp. 2551-2553.

[15]M. Keidar, and I. D. Boyd, "Plasma Flow and Plasma-Wall Transition in Hall Thruster Channel," *Physics of Plasmas*, Vol. 8, No. 12, Dec. 2001, pp. 5315-5322.

[16]Justin W. Koo, and Iain D. Boyd, "Computational Model of a Hall Thruster," *Computer Physics Communications*, Vol. 164, 2004, pp. 442-447.

[17]F. Taccogna, S. Longo, M. Capitelli, and R. Schneider, "Start-Up Transient in a Hall Thruster," *Contributions to Plasma Physics*, Vol. 46, No. 10, 2006, pp. 781-786.

[18]E. Ahedo, and J. Rus, "Vanishing of the Negative Anode Sheath in a Hall Thruster," *Journal of Applied Physics*, Vol. 98, 043306, 2005.

[19]V. V. Zhurin, H. R. Kaufman, and R. S. Robinson, "Physics of Closed Drift Thrusters," *Plasma Sources Science and Technology*, Vol. 8, 1999, pp. R1-R20.

[20]A. M. Bishaev, and V. Kim, "Local Plasma Properties in a Hall-Current Accelerator with an Extended Acceleration Zone," *Soviet Physics – Technical Physics*, Vol. 23, No. 9, Sept. 1978, pp. 1055-1057.

[21]Vladimir Kim, "Main Physical Features and Processes Determining the Performance of Stationary Plasma Thrusters," *Journal of Propulsion and Power*, Vol. 14, No. 5, 1998, pp. 736-743.

[22]L. Dorf, V. Semenov, Y. Raitses, and N. J. Fisch, "Hall Thruster Modeling with a Given Temperature Profile," *38th AIAA/ASME/SAE/ASEE Joint Propulsion Conference & Exhibit*, Jul. 2002, Indianapolis, Indiana.

[23]K-U Riemann, "The Bohm Criterion and Sheath Formation," *Journal of Physics D: Applied Physics*, Vol. 24, 1991, pp. 493-518.

[24]C. Boniface, L. Garrigues, G. J. M. Hagelaar, J. P. Boeuf, D. Gawron, and S. Mazouffre, "Anomalous Cross Field Electron Transport in a Hall Effect Thruster," *Applied Physics Letters*, Vol. 89, 161503, 2006.

[25]Leonid A. Dorf, Yevgeny F. Raitses, Artem N. Smirnov, and Nathaniel J. Fisch, "Anode Fall Formation in a Hall Thruster," AIAA-2004-3779, *40th AIAA/ASME/SAE/ASEE Joint Propulsion Conference & Exhibit*, Jul. 2004, Fort Lauderdale, FL.

[26]M. Mitchner, and Charles H. Kruger, Jr., "Partially Ionized Gases," John Wiley & Sons, Inc., New York, 1973, pp. 140.

[27]G. S. Kino, and E. K. Shaw, "Two-Dimensional Low-Pressure Discharge Theory," *The Physics of Fluids*, Vol. 9, No. 3, Mar. 1966, pp. 587-593.

[28]J. P. Boeuf, L. Garrigues, and L. C. Pitchford, "Modeling of a Magnetized Plasma: The Stationary Plasma Thruster," *Electron Kinetics and Application of Glow Discharge*, 1998, pp. 85-100.

[29]J. P. Boeuf, and L. Garrigues, "Low Frequency Oscillations in a Stationary Plasma Thruster," *Journal of Applied Physics*, Vol. 84, No. 7, Oct. 1998, pp. 3541-3554.

[30]Kybeom Kwon, "A Novel Numerical Analysis of Hall Effect Thruster and its Application in Simultaneous Design of Thruster and Optimal Low-Thrust Trajectory," Ph.D. Dissertation, School of Aerospace Engineering, Georgia Institute of Technology, Atlanta, GA, 2010.

[31]John M. Sankovic, John A. Hamley, and Thomas W. Haag, "Performance Evaluation of the Russian SPT-100 Thruster at NASA LeRC," IEPC-93-094, *23rd International Electric Propulsion Conference*, Sept. 1993, Seattle, WA, USA.

[32]Robert S. Jankovsky, and Chris McLean, "Preliminary Evaluation of a 10 kW Hall Thruster," AIAA-99-0456, *37th AIAA Aerospace Sciences Meeting and Exhibit*, January 1999, Reno, NV.

[33]David Manzella, Robert Jankovsky, and Richard Hofer, "Laboratory Model 50 kW Hall Thruster," AIAA-2002-3676, *38th AIAA/ASME/SAE/ASEE Joint Propulsion Conference and Exhibit*, 7-10 July 2002, Indianapolis, IN.

[34]Hofer, R. R., and Jankovsky, R. S., "A Hall Thruster performance Model Incorporating the Effects of a Multiply-Charged Plasma," AIAA 2001-3322, *37th AIAA/ASME/SAE/ASEE Joint Propulsion Conference and Exhibit*, Salt Lake city UT, July 2001.